Iranian Journal of Medical Physics

ijmp.mums.ac.ir

Myocardial Iron Overload Assessment with Automatic Segmentation of Cardiac MR Images based on Deep Neural Networks

Mohamad Amin Bakhshali[1*], Maryam Gholizadeh[2], Parvaneh Layegh[3], Saeid Eslami[1]

1. Department of Medical Informatics, School of Medicine, Mashhad University of Medical Sciences, Mashhad, Iran
2. Institute of Bioinformatics, University Medicine Greifswald, Greifswald, Germany
3. Department of Radiology, Imam Reza Hospital, School of Medicine, Mashhad University of Medical Sciences, Mashhad, Iran

ARTICLE INFO

Article type:
Original Paper

Article history:
Received: Jan 06, 2024
Accepted: Mar 16, 2024

Keywords:
Thalassemia Major
Iron Overload
Myocardium
Magnetic Resonance Imaging
Deep learning
Heavily T2 Weighted MRM

ABSTRACT

Introduction: Heart failure due to myocardial iron overload is one of the main causes of death in thalassemia major (TM) patients. Therefore, cardiac magnetic resonance (CMR) imaging method with a multi-echo sequence can be used to assess the iron overload of TM patients. This study aimed to evaluate the myocardial iron overload in TM patients with automatic left ventricular (LV) segmentation of CMR images.

Material and Methods: Thirty-six TM patients were selected to acquire CMR images and clinical data. Automatic LV segmentation was implemented with U-Net, an automatically adapted deep convolutional neural network based on U-Net. With the signal intensity of the LV segmented area, T2* value can be calculated at different echo times, a widely used and approved method to assess myocardial iron overload.

Results: The accuracy of LV segmentation as measured by intersection-over-union (0.95) was substantially higher than non-deep learning based methods and at par with other deep learning based methods like. In addition, our results indicate that the proposed method outperformed in assessing LV iron overload over other deep learning based methods in terms of negative predictive value, positive predictive value, and Jaccard.

Conclusion: Relying on these outcomes, the proposed method as a deep learning based model yields better LV segmentation and notably impacts assessing myocardial iron overload.

►*Please cite this article as:*
Bakhshali MA, Gholizadeh M, Layegh P, Eslami S. Myocardial Iron Overload Assessment with Automatic Segmentation of Cardiac MR Images based on Deep Neural Networks. Iran J Med Phys 2025; 22: 6-13. 10.22038/ijmp.2024.77319.2362.

Introduction

Thalassemia is a blood disorder that causes the body to make an abnormal form of hemoglobin, resulting in anemia from the excessive destruction of red blood cells [1]. The direct effects of thalassemia major (TM) on the body's organs and tissues are caused by the profoundly damaging effects of anemia and the by-products of hemolysis. Indirect effects include organ damage caused by iron overload following blood transfusions or blood-borne infections [2]. Iron losses are typically negligible, and a large percentage of the iron used for hemoglobin synthesis is heme iron derived from hemoglobin. Each blood transfusion introduces approximately 200 milligrams of iron into the body, and the body has no natural way of removing this amount of iron in a short time. With repeated blood transfusions, the amount of iron deposition in TM patients reaches about 20 times normal, resulting in iron overload [3]. Cellular self-destruction processes will begin if adequate treatment is not provided in these cases. The consequences of the destruction include a decrease in heart tissue function (systole or diastole), cardiac myocyte death, the onset of heart failure symptoms, and, eventually, patient death. The leading cause of death in TM patients associated with blood transfusions is heart failure caused by myocardial iron overload [4].

With early therapy, thalassemia patients with no myocardial iron overload symptoms can return to normal life. As a result, prompt diagnosis and interventions, such as adjusting the dosage of prescription medicine, have the potential to affect the outcome. It is challenging to detect patients at risk for heart failure early because the left ventricular function in thalassemia patients with iron deficiency may be normal long after the onset of heart failure [5]. Therefore, designing and developing a computer-aided diagnosis system capable of monitoring myocardial iron overload is essential.

Cardiac magnetic resonance (CMR) imaging provides significant information about the structure, function, and the location and nature of tissue damage in the heart, all of which can assist in determining various etiologies of cardiac injury [6]. T2*-weighted CMR imaging is a viable method for determining

*Corresponding Author: Tel: +98- 9126718442; Email: bakhshalima2@mums.ac.ir

myocardial iron overload. The CMR method is a gold standard for measuring cardiac indexes and assessing the amount of iron deposition in the heart because it can show changes in the volume of cardiac chambers during the cardiac cycle [7]. The non-uniformity of the magnetic field increases with increasing myocardial iron deposition, resulting in a decrease in signal proportional to the amount of iron deposition in that area. Consequently, T2* decreases in milliseconds. According to studies of myocardial iron deposition patterns, the ventricular wall deposition is more than the atria, and it has a significant correlation with whole heart iron deposition. For this reason, imaging centers examine iron overload in the ventricular wall [8].

T2*-weighted CMR images, geometric operations and active geodesic contours were used by Luo et al. (2015) to segment the left ventricular (LV) and assessing iron accumulation in TM patients [9]. The correct detection rate (true positive rate) and false positive rate of CMR images was 84 percent, and 53 percent respectively. In general, conventional image processing methods were used in this study to assess the feasibility of iron overload. Automatic LV segmentation was used by Wantanajittikul et al. (2016) to determine the amount of iron overload in TM patients [10]. All of these investigations need the use of an automatic LV segmentation approach as a first step in assessing iron overload. Automatic left ventricular segmentation faces some technical problems, including 1. The overlapping intensity distribution of cardiac organ pixels and background structures; 2. The variable forms of epicardial and endocardial contours in different cardiac slices and phases; 3. Background and myocardium structures suffer from severe asymmetries; 4. Border information is blurred, particularly in apical and basal slices; 5. Variability of images among institutions, people, or devices; 6. intrinsic noise of cardiac MR images [11].

Testing segmentation methods on small databases were one of the previous work's limitations. Prior knowledge of semi-automated and user-dependent methods was also required. The use of CMR image segmentation methods based on deep learning (DL) for this purpose was presented by some studies [12-17] and achieved impressive results in terms of accuracy. Automation and high accuracy are important points in all these methods. DL networks are being used to address most of the problems highlighted above.

Martini et al. (2022) introduced a DL-based approach for regional analysis of myocardial T2* distribution [18]. A U-Net architecture-based deep CNN was trained to segment multi-echo T2*-weighted images across various regions of CMR images. The results indicated no significant differences in segmental T2* values compared to manual measurements. However, there remains room for improvement in terms of segmentation accuracy and repeatability across all CMR sequences.

In this study, we evaluate cardiac iron overload in TM patients using an advanced DL network. We employ the U-Net architecture, which offers a standardized workflow without the need for extensive fine-tuning, making it easy to implement and potentially suitable for widespread clinical use. The following section provides a detailed description of the proposed method, including the CMR image dataset and the segmentation technique. The results are presented and compared with other methods in Section 3, followed by a discussion in Section 4 and conclusions in Section 5.

Materials and Methods

Data

The CMR images of 37 TM patients and 14 healthy subjects were used in this study. A non-probability and simple random sampling strategy were used to acquire images from February 2016 to January 2019, and for all subjects, echocardiographic data and cardiac dysfunction were collected. The study's objectives were explained to all subjects and written, and verbal informed consent was obtained. Interviews with the subjects and their records in the file were used to fill out the questionnaire form relating to demographic information and disease characteristics. The subjects had no clinical signs of heart disease and were comprised of 23 men and 27 women with a mean age of 24.18, a standard deviation of 5.560, and an average body surface area (BSA) of 1.7514 m^2 [19].

CMR imaging was performed using a 1.5 Tesla Siemens Avanto B17 in Qaem Hospital, Mashhad, Iran. The Body Matrix coil had six elements in these experiments. A single breath-hold multi-echo gradient sequence with retrospective gating in three slices of short axis (base, mid, and apex) and eight echo times was used to assess the value of iron overload in the myocardial. There were three cuts made this way: The first was between the papillary muscles (to assess iron deposition in the papillary muscles), the ventricular wall (which is the thickest part), and the other two were put at equal intervals above and below the first cut [19]. Exclusion criteria included: 1. Clinical signs of heart failure (shortness of breath, decreased activity, swelling of the hands and feet, swelling around the eyes, chest pain, and heart rhythm disorders), 2. Left ventricular systolic dysfunction (LVEF< 50%), 3. Arterial hypertension, 4. Renal failure, 5. Diabetes mellitus, 6. Pulmonary hypertension, 7. Addiction, 8. Heart valve diseases. Imaging with transfusion periods of patients was adjusted to one week after blood transfusion [19].

The multi-echo sequence parameters were as follows [20-21]: Position, Supine; number of echo times, 8; first echo time, 2.97 milliseconds (ms); last echo time, 21.68 ms; Flip Angle, 20°; Base resolution, 256; Phase resolution, 40%; Voxel size, 3.5×1.4×10 millimeters (mm); Slice Thickness, 10 mm; Phase Encoding Direction, A >> P; Phase Oversampling, 30%; Fat

Suppression, Fat Saturation; Concatenations, 1; field of view (FOV_{Read}), 359 mm; field of view (FOV_{Phase}), 75 mm.

Proposed Method

The left ventricle is first segmented in CMR images using U-net in this study. In this segmentation, the epicardial and endocardial edges of the left ventricle are identified to assess the level of myocardial iron overload. Then, to obtain T2* values, an area in the interventricular wall bounded by the epicardial and endocardial edges is identified, and the signal intensity (SI) of this range is determined for each echo time (TE), and the exponential decay curve of SI over time was plotted. Finally, the T2* values for each range are obtained using the following equation [22]:

$$Signal\ Intensity = ke^{-\frac{TE}{T2^*}} \quad (1)$$

Where, k is a constant value, and each TE represents an echo time. The value of T2* is inversely proportional to the slope of the decay curve line. The minimum normal amount of myocardial T2* is 20 ms, and as the amount of T2* decreases to less than that, LVEF decreases, and atrial volume increases at the end of systole and diastole. As a result, a time greater than 20 ms is considered no iron overload in the myocardia, while a time less than that is considered iron overload [22]. The accurate segmentation of the LV in CMR images was carried out automatically using U-net, and other steps to assess myocardial iron overload were implemented using MATLAB software (v. R2021b).

Preparing and data augmentation

CMR images were first prepared before LV images segmentation. All images are aligned based on image capture with the linear mutual information method [23] so that the heart (including the left and right ventricles) is in the center of the image. The entire heart area in the images is made in the same size using a square crop (size is 192×256 pixels). Cropping other areas and focusing on the desired area improves the DL network's accuracy and efficiency. Using MATLAB software and the Image Labeler toolbox, a radiologist meticulously delineated the endocardial and epicardial borders of the LV in images corresponding to the first, second, and third echo times for each short-axis slice. Additionally, slices affected by noise or poor quality were excluded from the analysis.

All input images are normalized in terms of grayscale distribution; therefore, the grayscale of the normalized images has Mean= 0 and SD= 1. In the segmentation, mean-variance normalization (MVN) is a simple and effective method that significantly improves the learning capacity of DL networks. To avoid over-fitting, the training data in this study were augmented with affine transformations such as rotation (90, 180, and 270 degrees), vertical and horizontal displacement.

U-net Architecture

Convolution neural networks (CNNs) are among the best methods for image segmentation, providing remarkable accuracy and performance in many areas of image processing and pattern recognition. CNN's training data is based on a supervised end-to-end learning approach and automatically feature learning [23-24]. Recent advances in CNN architectures such as AlexNet, VGGNet, GoogleNet, and ResNet have made CNN standard for whole image classification. In this study, A U-net (no new U-net) architecture to achieve accurate and reproducible segmentation [25].

Figure 1 illustrates the U-Net architecture employed in this study. U-Net is specifically designed for image segmentation tasks, particularly in the field of biomedical image analysis. The network derives its name from its distinctive U-shaped structure. Below is a detailed breakdown of the “U-Net” architecture: 1. Encoder Path: The network begins with a contracting path, similar to a standard CNN used for image classification. This path is tasked with capturing contextual information and extracting features from the input image. It comprises repeated blocks of two 3×3 convolutional layers, each followed by a rectified linear unit (ReLU) activation function. Batch normalization is typically applied after each convolutional layer to enhance training stability. Following each convolutional block, a 2×2 max pooling operation with a stride of 2 is performed to reduce spatial dimensions and expand the receptive field.

2. Bottleneck: The bottleneck of the U-Net architecture is the central part of the U shape. It consists of repeated convolutional blocks, but unlike the encoder, the spatial dimensions are not further reduced. This part helps in capturing high-level context information. 3. Decoder Path: The decoder path is the expansive part of the U-Net, and it is responsible for generating the segmentation mask. It is a mirror image of the encoder path, and its goal is to localize and refine the segmentation boundaries. The decoder path involves upsampling the feature maps using transposed convolutions (also known as fractionally strided convolutions or deconvolutions). This operation increases the spatial resolution of the feature maps. Concatenation is performed between the feature maps from the corresponding encoder and decoder blocks to provide detailed localization information. 4. Final Layer: The final layer typically consists of a 1×1 convolutional layer with a softmax activation function. This layer outputs a probability distribution over the classes for each pixel.

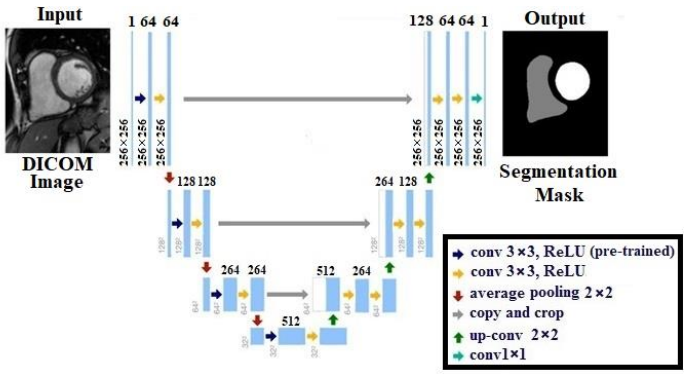

Figure 1. A schematic of U-net architecture proposed in this study

The key features of the U-Net architecture are its symmetric and U-shaped structure, skip connections that concatenate feature maps from the encoder to the decoder, and the use of transposed convolutions for upsampling. The skip connections help in preserving spatial information and gradients during training, which is crucial for accurate segmentation. The U-Net architecture has proven to be effective in various image segmentation tasks, particularly in medical imaging, where it has been successfully applied to tasks such as cell segmentation, organ segmentation, and tumor detection [25].

In this study, we also investigate the advantages of transfer learning to train the U-Net model using a limited number of images. Initially, the model was trained on the LV Segmentation Challenge (LVSC) database, which consists of 22,000 DICOM images. The dataset was divided into an 80-10-10 split: 80% for training, 10% for validation, and 10% for testing. The network training was conducted on a computer equipped with a 12-core Intel i7-7800 CPU running at 3.5 GHz, 64 GB of RAM, and an NVIDIA Titan Xp GPU with 12 GB of memory, operating on a Linux system. Experts provided LV images with defined contours, and the learning process was implemented in convolutional filters. For transfer learning, our U-Net model was initialized by transferring learned weights from the source model, specifically copying weights from selected convolutional and upsampling layers. The remaining layers were randomly initialized and fine-tuned through supervised training. In transfer learning, the initial learning rate (base_ir) is generally set to a low value, typically around 0.001.

Training protocol

The multinomial logistic loss on per-pixel softmax probabilities from input images and ground truths was minimized using stochastic gradient descent with a momentum of 0.9, parameter weights are randomly initialized. In addition, an L_2 weight decay regularization of 0.0005 and a dropout ratio of 0.5 were used to combat the effects of overfitting. The train was run for 1000 epochs, and the learning rate was calculated using the following equation:

$$Learning\ rate = base\_ir \times \left(1 - \frac{iter}{\max\_iter}\right)^{Power} \quad (2)$$

Where *base_ir* is the initial learning rate and is equal to 0.01. *iter* is the current number of iterations, and max_*iter* is the maximum number of iterations for the dataset. *Power* is 0.5 and to control the decay rate. Images of our dataset with data augmentation that mentioned before, were split into a training set (400 slices), validation set (50 slices), and test set (50 slices) for evaluation of performance.

Metrics

In this study, the following metrics are used to assess the accuracy and efficiency of the LV automated segmentation method using the ground truth as a reference. The Jaccard index is a metric that indicates the overlap or similarity between two areas that varies values from zero to unity. The zero value indicates a complete mismatch, and one indicates a perfect match with the ground truth. The Jaccard index is defined as:

$$J(A,M) = \frac{A \cap M}{A \cup M} = \frac{A \cap M}{A + M - (A \cap M)} \quad (3)$$

Where, *A* considered as an area in the main image and *M* considered as an area the ground truth that are compared with each other. Sensitivity (*p*), specificity (*q*), positive predictive value (PPV), and negative predictive value (NPV), are other metrics that are defined as:

$$p = \frac{T_1}{N_1},\ q = \frac{T_0}{N_0},\ PPV = \frac{T_1}{T_1 + F_1},\ NPV = \frac{T_0}{T_0 + F_0} \quad (4)$$

Where, T_1 and T_0 represent the number of correctly predicted pixels from the object and background area, while, F_1 and F_0 represent the number of incorrectly predicted pixels from the object and background area, respectively. The total number of pixels in the object area and background are N_1 and N_0, respectively.

Results

Results of LV segmentation using the proposed approach as well as other methods are reported in this section. To that end, the proposed method's results are compared with non-DL based methods (Geodesic active

contour (GAC) [9] and region growing algorithm [10]), as well as DL based method (U-Net [18]). All these mentioned methods were re-implemented. Although all the details of the methods may not have been considered, in regard that the focusing of this research is prediction of iron overload as opposed to segmentation performance. In addition, the results of iron overload evaluation using the proposed method are presented and compared with methods [9], [10], and [18].

Figure 2 (*a*) shows the two main raw images in the top and bottom rows, respectively. A radiologist's epicardial and endocardial contours are also visible in this figure (column *b*). Figure 2 (*c*) shows the segmented area created by the proposed method. Non-DL based methods (columns *d* and *e*) are the most prone to segmentation mistakes, while DL based method are the most accurate (columns *f*). In Figure 2 (*d-f*), the contours drawn outside the epicardial boundaries or inside the endocardial boundaries are incorrectly enclosed, resulting in an incorrect segmented area of the myocardial that is greater or less than its ground truth (column *b*).

The effectiveness of various methods in LV segmenting can be seen by using the metrics presented in Table 1. DL based methods achieve the highest segmentation accuracy, while non-DL based methods achieve the lowest segmentation accuracy. Our U-net model for predicting myocardial contours on the LV segmentation achieves the best scores in three out of five accuracy metrics, including the Jaccard, PPV, and NPV indexes and the values of *p* and *q* were closely equal to previous DL based methods. Note that our results were remarkably higher compared with non-DL based methods the value of five accuracy metrics.

Next, the amount of myocardial iron overload is evaluated based on the results of LV segmentation. The previous section's segmented area is divided into six equal areas by six lines at an angle of 60 degrees from each other (Figure 3). There is an intraventricular region and a ventricular wall in each of the areas. At all TEs, the ventricular wall SI was calculated, and the time-signal intensity curve was plotted (SI against TE). Then the curve will pass through all the obtained points using polynomial curve fitting. The decay slope of this curve is proportional to T2* time and was calculated from Equation (1).

Table 2 presents the measured T2* using the proposed method, methods [9] and [10]. These findings are based on the data collected from 36 TM patients [18]. Table 2 also includes clinical descriptions of some patients. As the results show, the T2* measured by the proposed method with clinical descriptions is very close, while the results are significantly different in the methods [9] and [10]. This difference is due to the myocardial segmentation method in [9] and [10] methods compared to the proposed method. Poor segmentation results strongly affect the measured T2* and cause a significant difference between it and the real size.

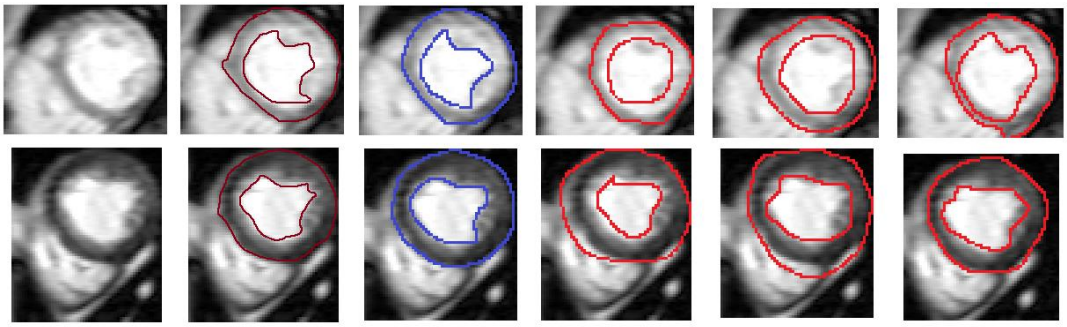

Figure 2. Differences of segmented areas in cardiac MR images using the proposed method and other methods. (a) Raw image, (b) Ground truth, (c) Proposed Method, (d) method [9], (e) method [10], (f) method [18].

Table 1. Comparison of different methods efficiency in LV segmentation, (Standard deviation)

Method	Type of Method	Jaccard	p	q	PPV	NPV
Method [9]	Non-DL based	0.64 (0.27)	0.53 (0.18)	0.67 (0.21)	0.50 (0.23)	0.56 (0.09)
Method [10]	Non-DL based	0.58 (0.23)	0.66 (0.20)	0.69 (0.19)	0.51 (0.14)	0.63 (0.12)
Method [18]	DL based	0.82 (0.09)	0.87 (0.11)	0.88 (0.12)	0.84 (0.80)	0.93 (0.09)
Proposed method	DL based	0.95 (0.11)	0.92 (0.14)	0.98 (0.02)	0.95 (0.09)	0.98 (0.02)

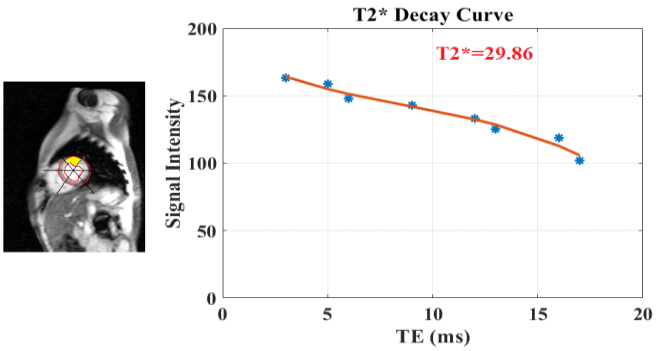

Figure 3. Curve fitting for T2* in the direction of one of the lines drawn of the myocardium

Table 2. T2* calculation results using the proposed method, method [9], [10], and [18] for all patients

Patient	T2* (ms) Proposed method	T2* (ms) Method [9]	T2* (ms) Method [10]	T2* (ms) Method [18]	Clinical description
Patient 1	38.9	35	30	36.5	high ferritin serum level
Patient 2	20.12	19	20	23	
Patient 3	12.6	13	22	18	with chelation therapy
Patient 4	30.56	32	30	30	
Patient 5	13.6	14	10	9	
Patient 6	28.9	32	25	22	
Patient 7	20.4	22	19	20	
Patient 8	4.09	3	7	5.5	high ferritin serum level
Patient 9	2.92	4	8	9	
Patient 10	3.7	4	8	3	high ferritin serum level
Patient 11	7.6	2	8	3	with chelation therapy
Patient 12	11.70	15	16	19	
Patient 13	11.90	14	15	16	
Patient 14	6.02	8	10	11	
Patient 15	6.52	9	9	10	high ferritin serum level
Patient 16	3.98	1	2	2.2	
Patient 17	41.02	37	29	28	
Patient 18	43.02	40	35	28	
Patient 19	36	32	31	30	
Patient 20	20	15	11	9	
Patient 21	13.85	19	12	11	
Patient 22	7.6	9	11	8	high ferritin serum level
Patient 23	27.03	20	15	19	
Patient 24	14.19	18	21	16	
Patient 25	5.5	7	10	8	high ferritin serum level
Patient 26	7	9	10	9	
Patient 27	34	38	39	35	
Patient 28	15.9	19	22	35	
Patient 29	39.9	35	35	30	
Patient 30	36.6	30	30	27	
Patient 31	5.2	6	8	7	
Patient 32	7.3	2	1	3	
Patient 33	6.5	3	3	7	high ferritin serum level
Patient 34	17.9	18	20	22	
Patient 35	2.1	1	5	3	
Patient 36	24.9	29	29	25	
Patient 37	14.3	10	10	12	with chelation therapy

Discussion

Deep learning image segmentation techniques provide high accuracy and facilitate subsequent steps to assess the amount of myocardial iron overload. In this study, for the first time, we used LV segmentation in CMR images by deep neural networks to assess the amount of myocardial iron overload in the TM patients. The proposed method's segmentation accuracy and speed improved by using the LVSC as transfer learning

in our model. Moreover, thoracic MRI scans and clinical data of thirty-seven TM patients who had myocardial iron overload were recruited for this study.

The presented DL-based method for LV segmentation and subsequent assessment of myocardial iron overload demonstrates notable advancements in accuracy and clinical relevance compared to several existing studies, as discussed in the introduction. In regarding to segmentation accuracy, Method [9] (GAC-based Segmentation) exhibits superior segmentation accuracy, achieving a Jaccard index of 0.95 and Jaccard index of 0.64. The proposed method's segmentation accuracy is consistently higher across various metrics, emphasizing its robustness in accurately delineating myocardial boundaries. In comparison, Method [10] (Region Growing Algorithm) achieves a lower Jaccard index (0.58) than both the proposed method and Method [9]. The proposed DL-based approach excels with a Jaccard index of 0.95, highlighting its superior segmentation performance.

According to iron overload assessment, T2* measurements obtained by the proposed method exhibit close alignment with clinical descriptions, emphasizing its reliability in assessing myocardial iron overload. In contrast, Method [18] shows significant differences in T2* values for several patients, suggesting potential limitations in accurately characterizing iron deposition in the myocardium. The proposed method's T2* calculations demonstrate closer agreement with clinical descriptions compared to Method [9] and [10]. The superior segmentation accuracy of the proposed DL-based approach contributes to more reliable T2* measurements, reducing discrepancies between predicted and actual iron overload.

The study's comprehensive evaluation, including visual comparisons, segmentation accuracy metrics, and clinical correlation of T2* values, underscores the proposed method's potential clinical applicability. The emphasis on accurate segmentation contributes to the reliable assessment of myocardial iron overload, offering valuable insights for early detection and intervention in thalassemia major patients. In summary, the presented study significantly advances the state-of-the-art in DL-based LV segmentation for assessing myocardial iron overload in thalassemia major patients. The achieved results surpass the accuracy of traditional methods and existing DL-based approaches, emphasizing the proposed method's potential as a robust and clinically relevant tool for enhancing diagnostic precision in this critical medical domain.

One of the limitations of this study was the limited number of CMR images of TM patients with the relevant clinical data, such as ferritin or transfusion index. Furthermore, the disturbance and noise in these people's images make image labeling quality difficult for radiologists. One of the other study's limits and challenges was the initial training of a large number of network weights and tuning the hyperparameters.

It is suggested that future research assess the myocardial iron overload using the proposed method at specific echo and compare the results. It is also proposed that these approaches assess the amount of atrium iron overload and its relevance to current findings. Since the heart rate of thalassemia patients due to chronic anemia is higher than normal, it is recommended that the volumes of the heart cavities be indexed to the patient's heart rate. In addition, to evaluate the myocardial iron overload, T1 and T2 mapping sequences could be used in MR, and the resulting images could be evaluated using the proposed methods. This proposed method could be utilized to develop a diagnostic aid software for radiologists and cardiologists. Research on various cardiac diseases that necessitate segmentation of a specific area of the myocardium, such as the left ventricle, can benefit from this research in the same way. Our study serves as a pilot for other methods that process CMR images.

Conclusion

In conclusion, our study introduces a novel approach for assessing myocardial iron overload in TM patients, utilizing deep learning-based LV segmentation on CMR images. The proposed method, employing the U-net architecture, showcases a significant advancement in accuracy and efficiency, surpassing traditional methodologies. Leveraging transfer learning from the LVSC database further enhances the segmentation accuracy and speed of our model.

Our findings demonstrate the superior efficacy of the proposed method in estimating myocardial iron overload compared to conventional approaches. Deep learning-based image segmentation proves to be a robust solution, outperforming non-deep learning methods, particularly crucial in the intricate patterns of myocardial MR images where precise LV segmentation is paramount.

Acknowledgment

The authors would like to express their gratitude to Mashhad University of Medical Sciences for the financial support of this project, with the following code of ethics: IR.MUMS.MEDICAL.REC.1400.730. This study was approved by the Research Ethics Committees of the School of Medicine, Mashhad University of Medical Sciences. The online version of the approval is available at the following address and is open to the public:

https://ethics.research.ac.ir/IR.MUMS.MEDICAL.REC.1400.730

References

1. Franke GN, Kubasch AS, Cross M, Vucinic V, Platzbecker U. Iron overload and its impact on outcome of patients with hematological diseases. Mol Aspects Med. 2020;75:100868. DOI: 10.1016/j.mam.2020.100868.
2. Fernandes JL. MRI for Iron overload in thalassemia. Hematol Oncol Clin North Am. 2018;32(2):277-95. DOI: 10.1016/j.hoc.2017.11.012.
3. Sarikouch S, Koerperich H, Boethig D, Peters B, Lots J, Gutberlet M, et al. Reference values for atrial

size and function in children and young adults by cardiac MR: a study of the German competence network congenital heart defects. J Magn Reson Imaging. 2011;33(5):1028-39. DOI: 10.1002/jmri.22521.
4. Wood JC, Enriquez C, Ghugre N, Otto-duessel M, Aguilar M, Nelson MD, et al. Physiology and pathophysiology of iron cardiomyopathy in thalassemia. Ann N Y Acad Sci. 2005;1054:386-95. DOI: 10.1196/annals.1345.047.
5. Vogel M, Anderson LJ, Holden S, Deanfield JE, Pennell DJ, Walker JM. Tissue doppler echocardiography in patients with thalassaemia detects early myocardial dysfunction related to myocardial iron overload. Eur Heart J. 2003;24(1):113-9. DOI: 10.1016/s0195-668x(02)00381-0.
6. Zareiamand H, Darroudi A, Mohammadi I, Moravvej SV, Danaei S, Alizadehsani R. Cardiac Magnetic Resonance Imaging (CMRI) Applications in Patients with Chest Pain in the Emergency Department: A Narrative Review. Diagnostics (Basel). 2023;13(16):2667. DOI: 10.3390/diagnostics13162667.
7. Fragasso A, Ciancio A, Mannarella C, Gaudiano C, Scarciolla O, Ottonello C, et al. Myocardial iron overload assessed by magnetic resonance imaging (MRI) T2* in multi-transfused patients with thalassemia and acquired anemias. Eur J Intern Med. 2011;22(1):62-5. DOI: 10.1016/j.ejim.2010.10.005.
8. Meloni A, Restaino G, Borsellino Z, Caruso V, Spasiano A, Zuccarelli A, et al. Different patterns of myocardial iron distribution by whole-heart T2* magnetic resonance as risk markers for heart complications in thalassemia major. Int J Cardiol. 2014;177(3):1009-12. DOI: 10.1016/j.ijcard.2014.09.139.
9. Luo Y, Ko JK, Guan Y, Li L, Qin J, Ha PA, et al. Myocardial iron loading assessment by automatic left ventricle segmentation with morphological operations and geodesic active contour on T2* images. Sci Rep. 2015;5:12438. DOI: 10.1038/srep12438.
10. Wantanajittikul K, Theera-Umpon N, Saekho S, Auephanwiriankul S, Phrommintikul A, Leemasawat K. Automatic cardiac T2* relaxation time estimation from magnetic resonance images using region growing method with automatically initialized seed points. Comput Methods Programs Biomed. 2016;130:76-86. DOI: 10.1016/j.cmpb.2016.03.015.
11. Petitjean C, Dacher JN. A review of segmentation methods in short axis cardiac MR images. Med Image Anal. 2011;15(2):169-84. DOI: 10.1016/j.media.2010.12.004.
12. Chen C, Qin C, Qiu H, Tarroni G, Duan J, Bai W, et al. Deep Learning for Cardiac Image Segmentation: A Review. Front Cardiovasc Med. 2020;7:25. DOI: 10.3389/fcvm.2020.00025.
13. Hu H, Pan N, Liu H, Liu L, Yin T, Tu Z, et al. Automatic segmentation of left and right ventricles in cardiac MRI using 3D-ASM and deep learning. Signal Process Image Commun. 2021;96:116303. DOI: 10.1016/j.image.2021.116303.
14. Xie L, Song Y, Chen Q. Automatic left ventricle segmentation in short-axis MRI using deep convolutional neural networks and central-line guided level set approach. Comput Biol Med. 2020;122:103877. DOI: 10.1016/j.compbiomed.2020.103877.
15. Vigneault DM, Xie W, Ho CY, Bluemke DA, Noble JA. Ω-Net (Omega-Net): Fully automatic, multi-view cardiac MR detection, orientation, and segmentation with deep neural networks. Med Image Anal. 2018;48:95-106. DOI: 10.1016/j.media.2018.05.008.
16. Abdeltawab H, Khalifa F, Taher F, Alghamdi NS, Ghazal M, Beache G, et al. A deep learning-based approach for automatic segmentation and quantification of the left ventricle from cardiac cine MR images. Comput Med Imaging Graph. 2020;81:101717. DOI: 10.1016/j.compmedimag.2020.101717.
17. Avendi MR, Kheradvar A, Jafarkhani H. A combined deep-learning and deformable-model approach to fully automatic segmentation of the left ventricle in cardiac MRI. Med Image Anal. 2016;30:108-19. DOI: 10.1016/j.media.2016.01.005.
18. Martini N, Meloni A, Positano V, et al. Fully Automated Regional Analysis of Myocardial T2* Values for Iron Quantification Using Deep Learning. Electronics. 2022;11:2749. DOI: 10.3390/electronics11172749.
19. Shiae Ali E, Bakhshali MA, Shoja Razavi SJ, Poorzand H, Layegh P. Cardiac MR images of thalassemia major patients with myocardial iron overload: a data note. BMC Res Notes. 2021;14:318. DOI: 10.1186/s13104-021-05733-2.
20. Nazarpoor M. Non-uniformity of Clinical Head, Head and Neck, and Body Coils in Magnetic Resonance Imaging (MRI). Iran J Med Phys. 2014;11(4):322-7.
21. Lotfi Marangaloo S, Ariamanesh AS, Aminzadeh B, Abedi H, Abbaszadeh A, Montazerabadi A. Comparison of Three-Dimensional Double-Echo Steady-State Sequence with Routine Two-Dimensional Sequence in the Depiction of Knee Cartilage. Iran J Med Phys. 2020;17(2):75-80.
22. Anderson LJ, Holden S, Davis B, Prescott E, Charrier CC, Bunce NH, et al. Cardiovascular T2-star (T2*) magnetic resonance for the early diagnosis of myocardial iron overload. Eur Heart J. 2001;22(23):2171-9. DOI: 10.1053/euhj.2001.2822.
23. Zhu YM. Volume image registration by cross-entropy optimization. IEEE Trans Med Imaging. 2002;21(2):174-80. DOI: 10.1109/42.993135.
24. Li Q, Li L, Wang W, Li Q, Zhong J. A comprehensive exploration of semantic relation extraction via pre-trained CNNs. Knowl Based Syst. 2020;194:105488. DOI: 10.1016/j.knosys.2020.105488.
25. Ronneberger O, Fischer P, Brox T. U-Net: Convolutional Networks for Biomedical Image Segmentation. In: Navab N, Hornegger J, Wells W, Frangi A, editors. Medical Image Computing and Computer-Assisted Intervention − MICCAI 2015. Cham: Springer; 2015. p. 234−41. DOI: 10.1007/978-3-319-24574-4_28.